Batteries & Supercaps

Research Article
doi.org/10.1002/batt.202300534

Chemistry Europe
European Chemical Societies Publishing

www.batteries-supercaps.org

Check for updates

Impact of Lithium-Ion Battery Separators on Gas Evolution during Temperature Abuse

Lars Bläubaum,[a] Philipp Röse,[a] Florian Baakes,[a] and Ulrike Krewer*[a]

Separators in lithium-ion batteries are typically considered to be electrochemically inert under normal operating conditions. Yet, temperature abuse tests at elevated temperatures of ca. 60 °C to 132 °C show that the choice of separator material has a decisive influence on battery behavior and degradation. Using online electrochemical mass spectrometry, we analyzed the evolution of cell voltage and gas products during and after thermal abuse for different separators. Polypropylene and polytetrafluoroethylene seem exhibited little change in gas evolution, producing only modest amounts of CO_2 and POF_3. In contrast, glass fiber and polyethylene terephthalate separators caused additional gas release, indicating electrochemical instability. Polyethylene terephthalate produced significantly more gas, resulting in the mechanical failure of the separator and drastic performance losses. The amount of CO_2 evolved with polyethylene terephthalate is four times higher than that of the glass fiber separator. However, the amount of POF_3 detected was five times higher for the glass fiber separator.

Introduction

The demand for lithium-ion batteries to deliver high energy and power density and, in particular, very short charging times leads to frequent operations near the limits of their stability windows. This results in increased load, material stress, risk of lithium plating, and high temperatures, all of which motivate intensive research regarding battery safety. The most significant safety issue with lithium-ion batteries is thermal runaway, a cascade of mostly exothermic reactions that can lead to fire or even explosive failure.[3] Thermal runaway is preceded by a self-heating phase, wherein exothermic reactions from the decomposition of cell components increase temperature. Countermeasures are required during this self-heating phase in order to prevent thermal runaway.[4] This requires a profound understanding of the reactions taking place. Various experimental methods are used to obtain insights into the processes during self-heating and thermal runaway, as well as to assess overall battery safety, such as, nail penetration, crush, and oven tests.[3c,5] All these tests typically increase temperature of the battery via various mechanisms, such as causing mechanical damage to induce short circuiting, resulting in exothermic decomposition reactions. Oven tests allow controlled temperature regulation and, thus, the investigation of specific reaction processes and their correlation with electrochemical behavior. At certain temperatures and phases, before and during self-

heating, capacity and voltage drop due to increased electrochemical reactivity, and pressure increases due to gas evolution from these reactions; see exemplary eq. 1–6.[6] Typically, the previously mentioned safety tests do not analyze the evolving gases. An analysis of the reaction gases, e.g., CO, CO_2, C_2H_4, and POF_3 in eq. 1–6, allows conclusions to be drawn about the degradation mechanisms of the electrolyte and the solid-electrolyte interphase (SEI). The SEI is a thin passivation layer on the carbon electrode, mainly reported to be composed of Li_2CO_3, $(CH_2OCO_2Li)_2$, and LiF.[6e,f] Some works suggest alternative species, such as, lithium ethylene mono-carbonate (LEMC).[7] Other studies report that LEMC requires water as a reactant, allowing it to only form in limited quantities. This makes LEMC unlikely to be a main component of the SEI.[8] We here keep with the frequently used decomposition reactions as a starting point for high-temperature gas analysis: The reactions (eq. 1–5) with the solvent ethylene carbonate (EC) or dimethyl carbonate (DMC), as well as the reaction of the conductive salt Lithium hexafluorophosphate ($LiPF_6$) are shown below:[9]

$$2C_3H_4O_3 \ (EC) \xrightarrow{+2 \ Li^+, \ 2e^-} (CH_2OCO_2Li)_2 + C_2H_4 \uparrow \tag{1}$$

$$C_3H_4O_3 \ (EC) \xrightarrow{+2 \ Li^+, \ 2e^-} Li_2CO_3 + C_2H_4 \uparrow \tag{2}$$

$$(CH_2OCO_2Li)_2 \longrightarrow Li_2CO_3 + C_2H_4 \uparrow + CO_2 \uparrow + 0.5O_2 \uparrow \tag{3}$$

$$C_3H_6O_3 \ (DMC) \xrightarrow{+2 \ Li^+, \ 2e^-} 2LiOCH_3 + CO \uparrow \tag{4}$$

$$C_3H_4O_3 \ (EC) \xrightarrow{+2 \ Li^+, \ 2e^-} (CH_2OLi)_2 + CO \uparrow \tag{5}$$

$$LiPF_6 + H_2O \rightarrow POF_3 \uparrow + LiF + 2HF \uparrow \tag{6}$$
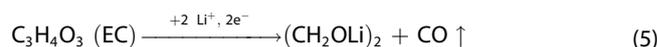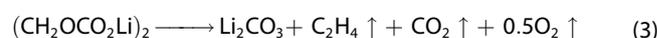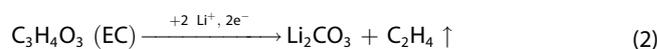
Several groups have investigated the impact of elevated temperatures up to 60 °C on gas evolution in lithium-ion batteries, by using online/operando/differential electro-chemical mass spectrometry (OEMS[10]/DEMS[11]).[12] They have also used offline methods, such as ion,[13] gas,[13–14] and liquid[15]

[a] Dr.-Ing. L. Bläubaum, Dr. P. Röse, F. Baakes, Prof. Dr.-Ing. U. Krewer
Institute for Applied Materials – Electrochemical Technologies
Karlsruhe Institute of Technology
Adenauerring 20b, 76137 Karlsruhe (Germany)
E-mail: ulrike.krewer@kit.edu

Batteries & Supercaps

Research Article
doi.org/10.1002/batt.202300534

Chemistry Europe
European Chemical
Societies Publishing

chromatography-mass spectrometry as well as infrared spectroscopy.[11b,16] Despite these works, there is little thorough battery degradation analysis at higher elevated temperatures available in literature. High temperature analysis is essential for understanding and improving safety behavior because the occurrence and type of degradation is strongly dependent on system temperature. Gasteiger and Nowak reported on the thermal decomposition of $LiPF_6$-based electrolytes at temperatures between 60 °C and 80 °C using OEMS and NMR spectroscopy (eq. 6).[1b,17] At temperatures of 60 °C to 110 °C, decomposition and reconstruction of the SEI occurs, leading to substantial evolution of C_2H_4 and CO (eq. 1–5). Further, the cathode-induced decomposition of the electrolyte and solvent begins near 150 °C due to oxygen release from the active material of the cathode.[3a,18] Due to the complexity of degradation reactions and evolving gases, we developed a physicochemical model that reveals the intricate reaction interactions and their resulting heat consumption and production that ultimately lead to self-heating behavior.[19] For instance, a pressure increase will inhibit solvent vaporization, causing a cooling effect during self-heating. So far, little attention has been paid to the influence of the separator on battery degradation reactions, as it is assumed that separators are inert toward electrode and electrolyte components. A widely accepted exception is borosilicate glass, which serves as a scavenger for HF.[1b] This lack of attention motivated us to examine the extent to which the various separators may affect the thermal stability of the electrolyte and electrode.

Separators that are typically employed in commercially available Lithium-Ion Batteries are microporous polyolefin membranes, such as polypropylene (PP) and polyethylene. These membranes have several architectures, ranging from single to multi-layer designs, which can be modified with ceramic coatings, like Al_2O_3 or TiO_2.[20] These coatings have low costs and are easily processable. Polyethylene in multi-layer design (PP-PE-PP) has an additional safety feature: it melts at ~130 °C, forming an insulating layer between the electrodes. This ultimately prevents further electrochemical reactions in the battery, and therefore inhibits self-heating behavior at these temperatures. In research, other materials, such as the borosilicate glass mentioned above and polyethylene terephthalate (PET) coated with Al_2O_3, and PTFE are frequently used. Impregnating the separator with Al_2O_3 increases the wettability and transport through the membrane. Further, it improves thermal conductivity and reduces the self-discharge by preventing shrinkage at elevated temperatures.[21]

Herein, we present the first, to our knowledge, operando gas analysis for lithium-ion battery cells at high temperatures up to 132 °C, in order to investigate the influence of separators with different chemical compositions used in commercial and experimental lithium-ion batteries. All of the separators used in this study are reported to be thermally stable outside the battery environment up to 132 °C. Yet, this stability changes strongly when using these separators in a battery setup. The analysis is conducted in a newly developed high-temperature online electrochemical mass spectroscopy (OEMS) setup for gas

analysis, which allows for the adjusting of temperature range, heating rate, voltage, and state of charge.

Results and Discussion

The following section describes the design and function of the newly developed high-temperature test cell (HTT cell). Further, we discuss the results of electrochemical characterization of lithium-ion batteries with four different separators during the temperature-induced stress test (TIS) up to 132 °C. This is followed by the measurements of reactant gases. The separators used in this investigation are a highly porous and thick borosilicate glass fiber (GF) separator, a thin Al_2O_3-coated polyethylene terephthalate (PET/Al_2O_3) separator with medium porosity, a thick polypropylene (PP) separator, and a thin highly porous polytetrafluoroethylene (PTFE) separator. For a detailed description of the experimental procedures, see the experimental section and SI.

High-Temperature Test Cell for Online Continuous Gas Measurements

Various experimental setups exist for simultaneous mass spectrometry and electrochemical characterization of battery cells. They were summarized in a review article by Dreyer et al.[22] Some battery cells extract the gas products through hydrophobic gas-permeable membranes,[11a,d] or discontinuously via a capillary. Others flush the cells with a carrier gas.[16b,23] Our setup uses a capillary connected to the interior of a battery cell via a by-pass system. Battery gases enter the by-pass system and are carried to the mass spectrometer by an argon gas flow. For the continuous measurements of battery performance and gases during regular operation at temperatures up to 132 °C, a battery cell was developed in collaboration with EL-Cell GmbH (Figure 1 and 4). It allows fast
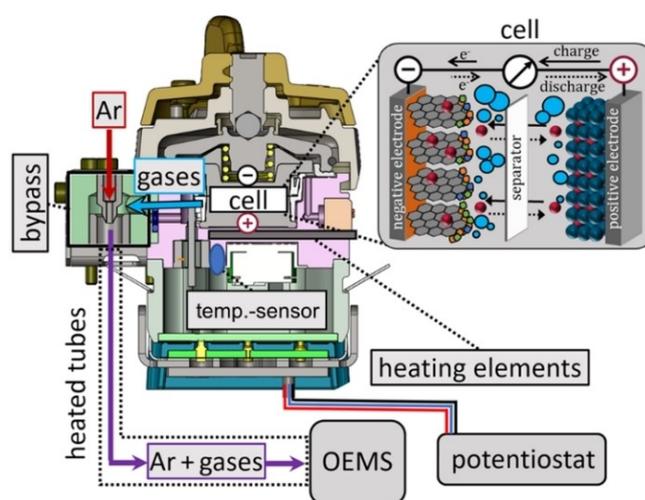
Figure 1. Design of the high temperature test cell for lithium-ion batteries its coupling to an online electrochemical mass spectrometer and potentiostat for analyzing gases and potential during operation and thermal heating.

Batteries & Supercaps

Research Article
doi.org/10.1002/batt.202300534

Chemistry Europe
European Chemical
Societies Publishing

homogeneous heating and gas sampling for electrochemical three-electrode measurements in a single-layered experimental cell format (PAT series test cell type). Temperature gradients across the electrochemical cell are negligible due to the placement of the heating elements close to the electrodes. Gas evolution quantities from thermal degradation reactions can be detected in near real-time over a wide temperature range. The same holds for time-resolved information about changes in cell voltage and current, as a function of temperature.

The main problem in conducting continuous high-temperature measurements at 60 °C to 132 °C arises from cell dry-out. This problem occurs especially with high vapor-pressure solvents, like dimethyl carbonate (DMC).[16b] In our HTT cell, significant drying out of the battery cell is avoided, since direct contact between argon carrier gas and liquid electrolyte is suppressed by the by-pass system. The battery cell design leads to a remarkably low loss of only 18 % from a 110 μL EC/DMC/ 1 M LiPF$_6$ electrolyte solution for 38 hours of operation. The sequence includes a ~28 h formation and a 10 h TIS along with 1 h exposure to 132 °C (~20 μL DMC loss by use of 110 μL electrolyte). To our knowledge, this is the first to report on the continuous high-temperature OEMS gas analysis of lithium-ion batteries up to 132 °C.

Electrochemical Behavior under Thermal Stress

To emulate thermal abuse, the cells were heated to 132 °C under open circuit conditions and at a state of charge of 50 % (heating ramp: 2 °C/min from ca. 25 °C); the temperature was held for 1 h, and then cooled down to ca. 25 °C. During the three-hour stress test and subsequent seven-hour resting phase at ca. 25 °C, the open circuit voltage (OCV) was monitored (Figure 2).

The cells with GF, PP, and PTFE separators exhibit only slight decreases in OCV during the stress test. The drop in OCV, which can be seen as a measure of self-discharge, is lowest for the GF cells compared to the other cells. It amounts to only about
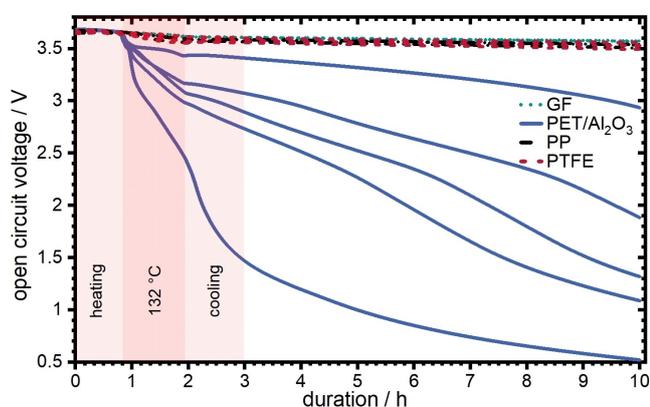
0.11 V in contrast to 0.13 ± 0.02 V and 0.14 ± 0.01 V for the PTFE and PP cells, respectively (Table 1).

In contrast, the cells with PET/Al$_2$O$_3$ separator, which are supposed to be thermally stable until ~200 °C, exhibit large and irreproducible drops in OCV with losses of ΔE^0 of 2.13 ± 0.91 V. The rapid drop in OCV starts at 132 °C but progresses significantly during the cooling and continues even during the resting phase. This behavior indicates that the common assumption that PET/Al$_2$O$_3$ is also an inert separator material at high temperatures, is incorrect.

To determine the degradation effect of the four separators on the lithium-ion battery, the cells were cycled once with C/10 between 4.2 V and 3.0 V after the temperature stress test (details see Table 4). The capacity of the batteries was determined from the discharge curves (Figure S2).

After the TIS, the discharge capacity (see Table 1) and the state of health (SOH$_{TIS}$) also varied strongly between the cells with the different separators. Again, PET/Al$_2$O$_3$ exhibited the most unpredictable behavior.

The cells with GF separators were the most temperature and stress-resistant, with 85 % of the capacity remaining after the stress test (SOH$_{TIS}$), followed by the PTFE (SOH$_{TIS}$ ~72 %) and PP cells (SOH$_{TIS}$ ~69 %). The most considerable capacity loss was observed for the PET/Al$_2$O$_3$ cells with a SOH$_{TIS}$ of ~34 %. The PET/Al$_2$O$_3$ cells were also found to be highly irreproducible. As no recovery of the OCV during cooling is observed, the decrease in OCV and SOH$_{TIS}$ should be attributed to a temperature and degradation-induced change in the state of charge as reported by Abdul-Quadir et al., and to irreversible decomposition reactions of the cell components.[24] In particular, organic SEI compounds such as (CH$_2$OCO$_2$Li)$_2$ decompose (eq. 3) in the applied temperature range up to 132 °C, starting at ca. 80 °C.[25] Decomposition reactions of the SEI produce gases and defects in the SEI.[26] This allows the inherently unstable electrolyte components to reach the surface of the negative electrode again and react with lithium to form new SEI species, such as (CH$_2$OCO$_2$Li)$_2$ (eq.1) or Li$_2$CO$_3$ (eq. 2). The consumption of lithium ions reduces the cell capacity, and thus OCV and total available capacity.

Figure 2. Open circuit voltage of cells with GF (green), PET (blue), PP (black), and PTFE (red) separators during the stress test. The number of analysed cells for GF, PP, and PTFE is n = 3; PET n = 5. The individual results of the tests are shown in Figure S3.

Table 1. Electrochemical changes due to the temperature stress test: OCV at begin of TIS (E$^0_{fresh}$), end of TIS (E$^0_{stressed}$), OCV difference $\Delta E^0 = E^0_{fresh} - E^0_{stressed}$, respective specific capacities before and after test (C$_{fresh/stressed}$) and change in state of health SOH$_{TIS}$ (= (C$_{stressed}$/C$_{fresh}$)·100 %).

	GF	PET/Al$_2$O$_3$	PP	PTFE
E$^0_{fresh}$/V	3.68 ± 0.00	3.68 ± 0.00	3.66 ± 0.01	3.66 ± 0.01
E$^0_{stressed}$[a]/V	3.57 ± 0.00	1.55 ± 0.92	3.52 ± 0.02	3.53 ± 0.03
ΔE^0/V[b]	0.11 ± 0.00	2.13 ± 0.91	0.14 ± 0.01	0.13 ± 0.02
C$_{fresh}$/ mAh g^{-1}	152.5 ± 0.6	152.2 ± 0.7	137.7	139.3 ± 5.7
C$_{stressed}$/ mAh g^{-1}	129.2 ± 1.0	52.4 ± 47.9	94.5	100.1 ± 13.0
SOH$_{TIS}$/%	84.7 ± 1.0	34.5 ± 31.5	68.7	71.7 ± 7.2

[a] OCV was measured after 10 h. [b] Mean value and standard deviations calculated from three cells for GF, PP (only two for specific capacity) and PTFE and five for PET/Al$_2$O$_3$.

Batteries & Supercaps

Research Article
doi.org/10.1002/batt.202300534

Chemistry
Europe
European Chemical
Societies Publishing

In the case of the PET/Al_2O_3 cells, it should be noted that two of the five cells did not exhibit typical charging behavior after the stress test and, no longer reached the final charging voltage of 4.2 V. Therefore, these cells were considered wholly broken down, and a SOH_{TIS} of 0% was assumed. None of the cells with other separators showed such a drastic behavior; we can conclude that the separator has been seriously damaged or inflicted severe damage on the other cell components. The work of Klein et al. and Homann et al. also reported PET-containing cells with atypical charging behavior and attributed this to micro-shorts.[2] It is, therefore, conceivable that a micro-short circuit could also cause the atypical charging behavior in PET/Al_2O_3 cells due to cracks in the 25 μm thick separator leading to direct contact of the negative and positive electrode (Figure S4).[27] In addition, Buechele et al. report that PET can react in the presence of DMC, residual water, and the SEI component lithium methoxide to form the redox active dimethyl terephthalate, therefore cleaving the polymer chain of PET/Al_2O_3.[28] The stress test temperature accelerates such PET decomposition: the hydrolysis of PET between 100 °C and 120 °C proceeds about 10,000 times faster than purely thermal decomposition.[29] Consequently, the PET/Al_2O_3 separator within Li-ion batteries could cause the battery breakdown at temperatures significantly below the typically assumed stability range of PET up to 250 °C.

Gas Evolution During Formation and Stress Test

The gas evolution of cells with different separator types is analyzed and discussed in the following section, in order to obtain knowledge of which decomposition reactions may have caused the strongly different performance losses during thermal abuse. The quantities of H_2, CH_4, C_2H_4, CO, O_2, CO_2, and POF_3 gas produced during the formation and TIS are shown in Figure 3a and b. They were obtained from time-resolved mass spectra (Figures 3c–f). The semi-quantitative gas quantities were calculated using a proportionality function and external calibration (see SI) from the mass spectra.

To see whether similar processes occur during the SEI formation at room temperature, as occurred within the stress test, we compared them to the gases produced during formation (Figure 3a). The approximate mean gas amounts during formation are similar for all separator types, with most detected gases being H_2 and C_2H_4. The PP separator cells had larger deviations for H_2 and C_2H_4. The produced gas amounts were very low for CH_4, CO, and CO_2 with quantities below 0.3 μmol, and are similar for all four separator types. Due to the only marginal differences in gassing between the cells with different separators, we consider SEI formation to be unaffected by the separator materials and deem the separators chemically inert under normal conditions – at least during the first cycles.

During the TIS, gas quantities were up to 30 times higher and deviated more between the separator types. Additional gas components compared to those observed during SEI formation were found, notably O_2, POF_3, and DMC (Figure 3b). The detection of DMC is attributed to the evaporation of the solvent in the electrolyte and is independent of the separator type. The main gas products detected are: H_2, as during SEI formation, as well as large quantities of CO_2 and POF_3. The other detected gases, CH_4, C_2H_4, CO, and O_2, are relatively low in quantity. Similar amounts of C_2H_4 were found during SEI formation. Thus, besides the SEI formation reactions, the high temperature triggers significant amounts of additional reactions.

Differences between the various separator types are largely limited to a few gases: CO_2 and POF_3. Generally, the PP and PTFE separators produced similar and mostly lower amounts of these gases than GF and PET/Al_2O_3. As the thermal decomposition of the separators would release gases, the similar and lower gas amounts detected for PP and PTFE suggest that these separators' significant chemical decomposition did not occur. Differences become apparent for GF and PET/Al_2O_3. PET/Al_2O_3
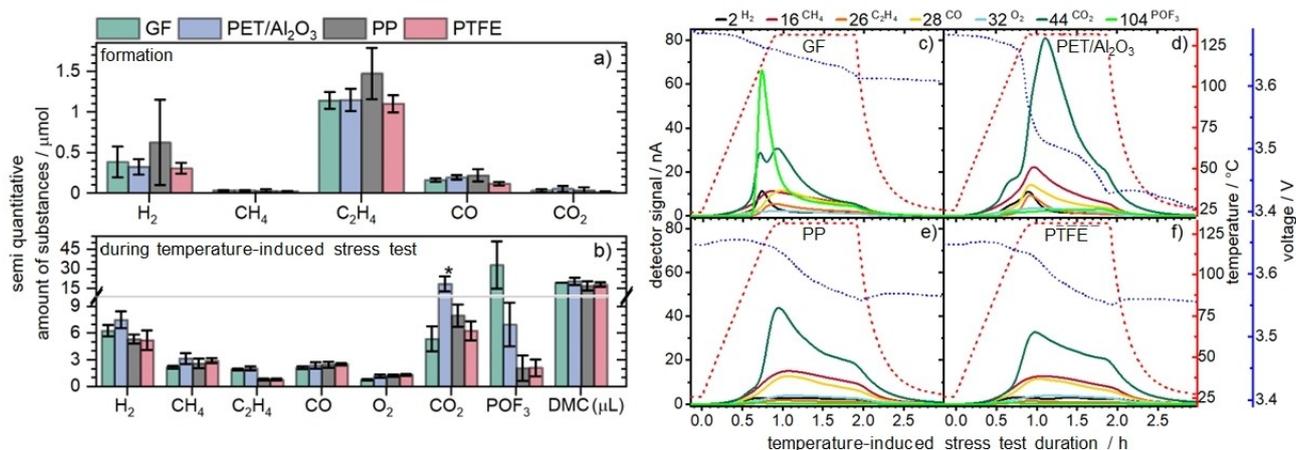
Figure 3. Semi-quantitatively determined gas amounts of the separator cells during a) the formation and b) stress test; the amount was calculated by employing a proportionality function incl. baseline correction, smoothing and external calibration (cf. SI); For comparison, the evaporated DMC quantity is shown in μL. Mean values and standard deviations are calculated from 3 cells for GF, PP and PTFE and 5 for PET/Al_2O_3. * Quantities for CO_2 with PET/Al_2O_3 may contain contributions of the PET-decomposition product acetaldehyde (m/z = 44).[2] c–f) Time-resolved mass spectra calculated by the proportionality function incl. baseline correction and smoothing, as well as temperature profile and cell voltage during TIS for the different separator materials.

Batteries & Supercaps

Research Article
doi.org/10.1002/batt.202300534

Chemistry Europe
European Chemical
Societies Publishing

separator cells showed four times more CO_2 evolution than cells with GF and the other separators: whereas the GF separator yielded a considerable amount of POF_3.

Considering that all neat separators are temperature stable up to 132 °C (Figure S5) and are considered inert during SEI formation, these results show that even at elevated temperatures up to 132 °C the composition of separators plays an important role in the evolution of gases, and thus also in the safety of lithium-ion battery.

This becomes particularly obvious when considering the CO_2 release in cells with PET/Al_2O_3 separators during decomposition. Marshall et al.[30] and Holland et al.[31] studied the thermal decomposition of neat PET and reported that CO, CO_2, and acetaldehyde are produced between about 280 °C and 370 °C. Similarly, Venkatachalam et al. reported that the thermal decomposition of neat PET starts above 250 °C, and gases such as CO, CO_2, acetaldehyde, or even C_2H_4 are formed in addition to many non-gaseous decomposition products.[29a] It seems that the conditions in a lithium-ion battery lead to polymer decomposition even at lower temperatures, as they did in our study. Here, the membranes are exposed to the electrolyte, low and high potentials, as well as the cathode and anode materials.

The temperature-dependent stability differences relating to the neat separator conditions are also evident when comparing cells with PET/Al_2O_3 and GF, considering their POF_3 release. POF_3 is a decomposition product of the conducting salt $LiPF_6$ (eq. 6). Al_2O_3 may have triggered such a chemical reaction. Multiple reports mention a thermally favored Al_2O_3 fluorination with HF up to 400 °C,[32] which takes place with the elimination of water (Scheme 1). The water formed in this process can promote hydrolysis reactions under the production of H_2.[12b,29,33] Gasteiger and coworkers reported that for lithium-ion batteries with PP separators, the H_2 evolution at the negative electrode is due to the reduction of trace water and protic electrolyte species from the cathode.[34] However, this process cannot explain the differences observed between the four separators, as all cells use the same electrolyte. We recently presented a thermal runaway model highlighting the negative impact of water impurities on battery lifetime and a cycle between HF and H_2O production.[35] Water may decompose with $LiPF_6$ forming POF_3 and HF; HF decomposes with Li_2CO_3 into CO_2, LiF, and water. This adds another reaction pathway for SEI
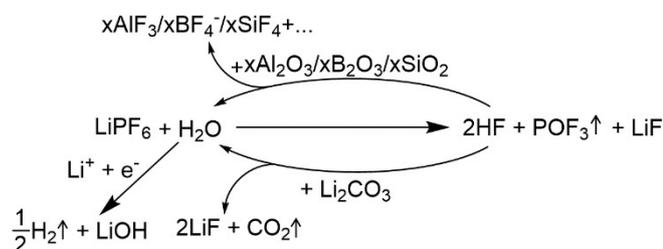
degradation besides a water source. Finally, HF may produce water again by reaction with the Al_2O_3-coated separator, which is a separator-specific reaction. Thus, a decomposition cycle can occur. This process is interrupted by water reduction to H_2 at the negative electrode.

A similar reaction scheme may be expected for cells with a GF separator composed of borosilicate glass (B_2O_3, SiO_2). It is known that when borosilicate glass is used, accelerated aging of the electrolyte takes place from about 80 °C to 85 °C, and HF reacts with the borosilicate glass to form water.[1b,c] Decomposition via these degradation pathways occurs only to a minor extent at 25 °C. Significant POF_3 release is only observed at 80 °C and above (Figure 3c, d). This explains the extraordinarily high amount of released POF_3 observed during the TIS of the cell with PET/Al_2O_3 and GF separators.

Likewise, the slightly higher H_2 amounts in the GF and PET/Al_2O_3 cells can be attributed to the increased water evolution and subsequent H_2 evolution reactions due to the degradation pathways.[1]

In conclusion, some separator materials can become unstable at elevated temperatures, even within their normal stability window, due to reactivity with battery components (cf. Figure S4). The separator type can strongly influence the thermal decomposition reactions and, thus, safety. The high reactivity of PET/Al_2O_3 may explain the above-reported cell failure and separator brittleness. In the worst case, it may lead to a short circuit and a strong sudden discharge. This can cause significant heat generation, which can lead to thermal runaway.

Conclusions

This study reveals the influence of different separators on the electrochemical gassing behavior of lithium-ion batteries during temperature-induced stress tests (TIS). To realize this, gas analyses were carried out with an online electrochemical mass spectrometric system that enables continuous measurements at temperatures up to 132 °C.

This unique approach of simultaneous acquisition of electrochemical measurements and operando gas analysis at high temperatures allows for the first time the comparison of the influence of cell composition with a variation in separators. Prior to the TIS, the batteries demonstrated similar electrochemical and gassing behavior. Under such typical battery formation and operation conditions, the investigated separators are chemically inert and are unlikely to have a significant influence on the SEI formation mechanism. However, the separator materials significantly impact electrochemical performance and gas evolution during the thermally induced stress test.

PP and PTFE separators showed similar gas evolution patterns and amounts of gases and similar performance losses, implying chemical robustness. In contrast, GF and PET/Al_2O_3 separators displayed increased gas production, particularly of CO_2 and POF_3, suggesting significant reactivity and involvement in the degradation reactions. Thus, the separators are not inert at these high temperatures. The increased POF_3 quantity is

Scheme 1. Glass fiber and PET separator-based degradation cycles: Reaction pathways triggered by water-induced conductive salt decomposition to POF_3 in the presence of alumina and borosilicate glass and SEI component Li_2CO_3 extracted from literature.[1]

Batteries & Supercaps

Research Article
doi.org/10.1002/batt.202300534

Chemistry Europe
European Chemical
Societies Publishing

attributed to the conductive salt decomposition; where borosilicate glass (GF) or Al_2O_3 (PET/Al_2O_3) convert HF into H_2O, which decomposes the conductive salt into further HF and POF_3. Remarkably, the reactivity of the GF separator did not significantly affect the cell's performance because it exhibited the highest state of health.

In contrast, PET/Al_2O_3 cells exhibited severe performance decreases and highly unreproducible electrochemical and gassing behavior. The study identifies significant decomposition of PET, indicated by high CO_2 production, and Al_2O_3, indicated by high POF_3 production, leading to a strong self-discharge. Notably, whereas it was previously claimed that Al_2O_3 coatings improve safety by preventing dendrites and reducing self-discharge, our studies clearly show that Al_2O_3-coated PET separators are detrimental to thermal safety as Al_2O_3 is expected to generate reactive water and significant amounts of gas.

The results underscore the importance of studying battery materials in their operating environment and under TIS for use and safety evaluations. Predictable and reproducible behavior in temperature studies in the range up to 130 °C are crucial, because they can start the self-heating phase leading to a thermal runaway.

Experimental Section

Material and Equipment

A high-temperature test cell (HTT Cell, PAT series test cell type, EL-Cell GmbH) was used for all experiments. Electrodes were purchased from CustomCells Itzehoe GmbH. The negative electrode has an area capacity of 2.2 mAh cm^{-2} with the following loading: 96 wt% SMG104 graphite active material, 2607SMG104. The capacity of the active material is 350 mAh g^{-1}. It contained further styrene-butadiene-rubber/carboxymethyl cellulose (SBR/CMC) and conductive additives, all applied on copper foil; the positive electrode has an area capacity of 2.0 mAh cm^{-2}, with the following loading: 93.5 wt% NMC 622 active material, K-771, with a capacity of the active material at 160 mAh g^{-1}. It further contained polyvinylidene fluoride and conductive additives, all applied on aluminum foil. EC:DMC electrolyte (1:1 / v:v,1 M LiPF$_6$, battery grade, Sigma Aldrich) was used. All electrodes were punched out to receive sheets with a uniform diameter of 18 mm. Their weight was measured (XS205, Mettler Toledo), and they were dried overnight at 120 °C under high vacuum before being transferred into an Ar glovebox (water and oxygen content under 0.1 ppm). All capacities were calculated based on the measured weight of the assembled electrodes.

The separator compositions were as follows: borosilicate glass (Whatman GF/A, porosity 91%, thickness 260 μm, m.p. > 300 °C), polyethylene terephthalate/Al_2O_3 (Viledon FS 3005–25, porosity 55%, thickness 25 μm, m.p. ~250 °C), polypropylene (Celgard 4560, porosity 55%, thickness 110 μm, m.p. ~150 °C), and polytetrafluoroethylene (Omnipore JVWP04700, porosity 88%, thickness 30 μm, m.p. ~300 °C). The HTT test cells contain the four separators mentioned above as sheets with a diameter of 21.6 mm. The cells were assembled in a glovebox under an Ar atmosphere, according to literature.[36] Temperature-stable separator housings and sealing ring materials made of polyether ether ketone (PEEK) were used for the selected temperature range.

Gases used for calibration were purchased from Air Liquide or Westfalen AG. The quantities and purities of the gases were: Ar (99.999%); calibration gas 1: Ar (main component, 99.999%), CH_4 (5025 ppm, 99.5%), C_2H_4 (5025 ppm, 99.5%) and CO_2 (5025 ppm, 99.5%); calibration gas 2: Ar (main component, 99.999%), H_2 (5005 ppm, 99.999%), CO (4991 ppm, 99.0%) and O_2 (4700 ppm, 99.999%). Chemicals used for calibration were purchased and used without further purification: dimethyl carbonate (99% dry, Acros Organics), Lithium hexafluorophosphate (99.99%, Sigma Aldrich), and Lithium peroxide (95%, ABCR). The conductive salt decomposition gas POF_3 is calibrated. This is done by *in situ* reaction of $LiPF_6$ with Li_2O_2 in the HTT cell under heating according to reaction eq. 7:

$$LiPF_6 + Li_2O_2 \xrightarrow{50\,°C} 3LiF + \frac{1}{2}O_2\uparrow + POF_3\uparrow \tag{7}$$
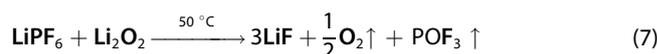
Setup for Temperature-induced Stress Test and Electrochemical characterization

The operando electrochemical and gas analysis setup couples a potentiostat and mass spectrometer (OEMS, see Figure 4). The HTT cell (EL-Cell) connects the lithium-ion battery with quick connectors with a heated transfer line and the mass spectrometer. Table 2 shows the parameters of the mass spectrometer (MS, Omnistar GSD 320, Pfeiffer Vacuum). The test conditions during the high-temperature abuse are shown in Table 3.

All assembled cells were cycled with a Gamry potentiostat (5000 E) in a self-built temperature chamber at 25 °C in the voltage range between 3.0 V and 4.2 V. The cycling procedure was identical for all experiments and is given in Table 4.

Table 2. Parameters of the mass spectrometer.

Parameter	Value
Multiple Ion Detection (MID)	m/z: 2, 16, 18, 26, 27, 28, 30, 32, 36, 44, 67, 69, 77, 78, 85, 88, 90, 104, 107, 118, 126, 155
Energy of the electron beam	70 eV
Detector	C-SEM
Capillary temperature	200 °C
Input heating	120 °C
Scan rate	500 ms
Ar flow rate	0.65 mL min^{-1}

Table 3. Heating profile of the HTT cell during TIS.

Parameter	Value
Start temperature	25 °C
Heating rate	2 °C min^{-1}
Test temperature	132 °C
Hold temperature at test temperature while recording the open-circuit voltage	60 min
End temperature	25 °C
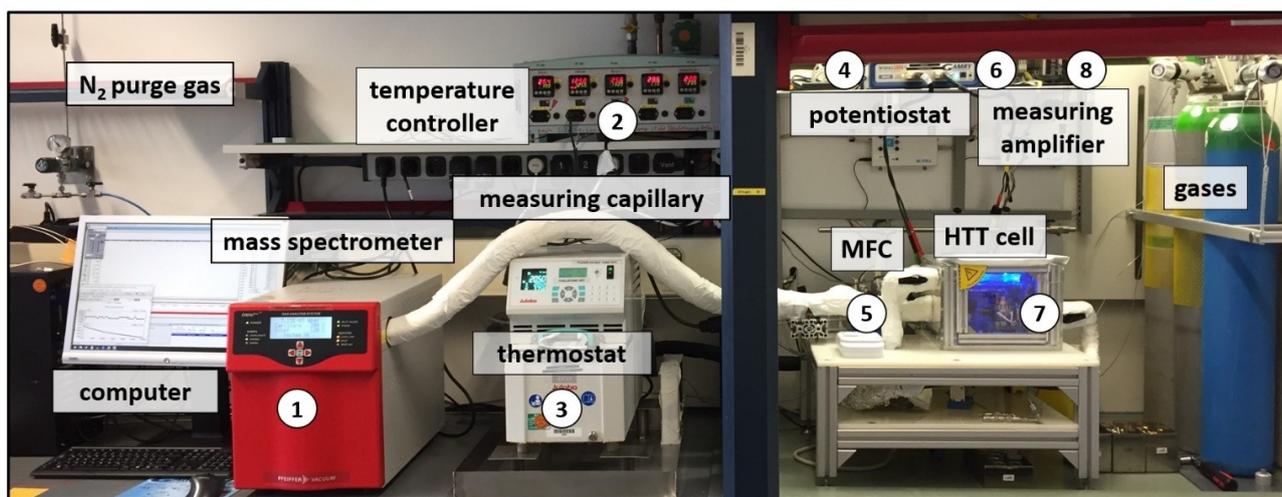
Figure 4. Setup of the high-temperature OEMS measuring system; 1) Omnistar GSD 320 OC2 (PTM81217121), Pfeiffer Vacuum, 2) N480D, B+B Sensors, 3) CF 31, Julabo, 4) Gamry Interface 5000, Gamry Instruments, 5) MFC: mass flow controller, EL-Flow Prestige FG-200 CV10, Bronkhorst, 6) Jumpflex 857–400, Wago, 7) HTT cell, EL-Cell, 8) Jumpflex 857–819, Wago.

Table 4. Cycling procedure for the temperature-induced stress test.

Parameter	Value
Temperature	25 °C
Rest time	6 h
Formation, 1 cycle	C/10
Heating step after formation starts at ~3.7 V (~SOC 50 %)	OCV for 10 h
Cycle after temperature induced stress test	C/10
Charge/Discharge	CC+CV/CC
U(cut-off)	4.2 V/3.0 V

OEMS Analysis of Battery Gases

For the OEMS analysis, it is assumed that only Ar, H_2, CH_4, C_2H_4, CO, O_2, CO_2, and POF_3 as well as DMC are present in the sample. The m/z signal was processed after measurement by baseline correction and smoothing. For the determination of the analytes, the measurement signals are corrected by using a proportionality function (eq. 8):

$$I_{m/z}^{i} = I_{m/z} - \underbrace{\sum_{j \neq i}\left(I_{m/z}^{j} \cdot \chi_{m/z}^{j}\right) - B_{m/z}}_{f(\chi_i)} \tag{8}$$

where I^i is the species of interest, $I_{m/z}$ the total ion current of the sum of I^i, I^j, and B of the m/z value, I^j the current signal of other (interference) species j, $\chi_{m/z}^{j}$ the proportionality factor, $B_{m/z}$ the background signal of the m/z value, and $f(\chi_i)$ the Proportionality function (see also Table S1). From the resulting OEMS signal proportions, the gas quantities of each analyte are determined approximately by external calibration (cf. Figure S1). Note that it cannot be excluded that additional species j are present in the samples and interfere with the m/z-values. Even a minimal deviation of the determined proportionality factor $\chi_{m/z}^{j}$ can lead to false conclusions when using the evaluation by the proportionality function. It is not physically feasible that a negative signal or a negative analyte quantity is present. Since such a circumstance can mean an overestimated relative intensity of the fragmentation behavior, the following condition is set for determining the proportionality factors $\chi_{m/z}^{j}$ in addition to the basis of the respective fragmentation pattern: The result of the proportionality function $f(\chi_i)$ must not become smaller than zero. A negative value due to a too high proportionality factor $\chi_{m/z}^{j}$ is corrected until zero. However, a compromise is made here since the decrease of the factor could cause the signal intensity of the analyte $I_{m/z}^{i}$ to be overestimated and, thus, the resulting amount of substance to be calculated too high. Under the same experimental conditions, similarly evaporated DMC quantities, and constant proportionality factors $\chi_{m/z}^{j}$ an equal systematic error can be assumed for all. With the additional assumption that only the gases Ar, H_2, CH_4, C_2H_4, CO, O_2, CO_2, and POF_3, as well as DMC, are present in the analysis matrix, the results can be evaluated semi-quantitatively relative to each other. At this point, it is noted that in terms of measurement accuracy, among other things, the correctness of the measurement (validation parameter) due to these assumptions and possible systematic errors must be checked.

Supporting Information

The supporting information contain following information: Table S1: overview of the calculations of the proportionality function; Figure S1: OEMS calibration curves; Figure S2: discharge curves before and after temperature-induced stress test; Figure S3: detailed OCV curves during temperature-induced stress test; Figure S4: microscopic images of the separators before and after use; Figure S5: differential scanning calorimetry measurements of the separators.

A part of the manuscript's content has been previously published in Lars Bläubaum's doctoral thesis doi:10.5445/IR/1000161140. Additional references are cited within the Supporting Information (Ref. [29b]).

Batteries & Supercaps

Research Article
doi.org/10.1002/batt.202300534

Chemistry
Europe

European Chemical
Societies Publishing

Conflict of Interests

The experimental high temperature test cell in the manuscript was developed in collaboration with EL-CELL GmbH.

Data Availability Statement

The data that support the findings of this study are openly available in KITopen repository at doi:10.35097/1857, reference number 1000165727.

Keywords: Separator degradation · Online electrochemical mass spectrometry · Gas analysis · Electrolyte decomposition · Battery safety

[1] a) A. T. S. Freiberg, J. Sicklinger, S. Solchenbach, H. A. Gasteiger, *Electrochim. Acta* **2020**, *346*, 136271; b) S. Wiemers-Meyer, S. Jeremias, M. Winter, S. Nowak, *Electrochim. Acta* **2016**, *222*, 1267; c) V. Kraft, W. Weber, M. Grützke, M. Winter, S. Nowak, *RSC Adv.* **2015**, *5*, 80150; d) S. J. An, J. Li, C. Daniel, D. Mohanty, S. Nagpure, D. L. Wood, *Carbon* **2016**, *105*, 52; e) S. F. Lux, J. Chevalier, I. T. Lucas, R. Kostecki, *ECS Electrochem. Lett.* **2013**, *2*, A121; f) S.-T. Myung, K. Izumi, S. Komaba, Y.-K. Sun, H. Yashiro, N. Kumagai, *Chem. Mater.* **2005**, *17*, 3695; g) Y. Tesfamhret, R. Younesi, E. J. Berg, *J. Electrochem. Soc.* **2022**, 010530.

[2] a) S. Klein, P. Bärmann, T. Beuse, K. Borzutzki, J. E. Frerichs, J. Kasnatscheew, M. Winter, T. Placke, *ChemSusChem* **2021**, *14*, 595; b) S. Klein, P. Harte, S. van Wickeren, K. Borzutzki, S. Röser, P. Bärmann, S. Nowak, M. Winter, T. Placke, J. Kasnatscheew, *Cell Rep. Phys. Sci.* **2021**, *2*, 100521; c) G. Homann, L. Stolz, K. Neuhaus, M. Winter, J. Kasnatscheew, *Adv. Funct. Mater.* **2020**, *30*, 2006289; d) G. Homann, L. Stolz, M. Winter, J. Kasnatscheew, *iScience* **2020**, *23*, 101225.

[3] a) R. Spotnitz, J. Franklin, *J. Power Sources* **2003**, *113*, 81; b) P. Ping, Q. Wang, P. Huang, J. Sun, C. Chen, *Appl. Energy* **2014**, *129*, 261; c) V. Ruiz, A. Pfrang, A. Kriston, N. Omar, P. van den Bossche, L. Boon-Brett, *Renewable Sustainable Energy Rev.* **2018**, *81*, 1427; d) X. Liu, D. Ren, H. Hsu, X. Feng, G.-L. Xu, M. Zhuang, H. Gao, L. Lu, X. Han, Z. Chu, J. Li, X. He, K. Amine, M. Ouyang, *Joule* **2018**, *2*, 2047.

[4] S. Shahid, M. Agelin-Chaab, *Energy Convers. Manage.* **2022**, *16*, 100310.

[5] Y. Chen, Y. Kang, Y. Zhao, L. Wang, J. Liu, Y. Li, Z. Liang, X. He, X. Li, N. Tavajohi, B. Li, *J. Energy Chem.* **2021**, *59*, 83.

[6] a) A. M. Andersson, K. Edström, *J. Electrochem. Soc.* **2001**, *148*, A1100; b) G. Gachot, S. Grugeon, M. Armand, S. Pilard, P. Guenot, J.-M. Tarascon, S. Laruelle, *J. Power Sources* **2008**, *178*, 409; c) H. Ota, Y. Sakata, A. Inoue, S. Yamaguchi, *J. Electrochem. Soc.* **2004**, *151*, A1659; d) M. N. Richard, J. R. Dahn, *J. Electrochem. Soc.* **1999**, *146*, 2068; e) T. Melin, R. Lundström, E. J. Berg, *Adv. Mater. Interfaces* **2022**, *9*, 2101258; f) R. Lundström, N. Gogoi, X. Hou, E. J. Berg, *J. Electrochem. Soc.* **2023**, *170*, 040516.

[7] a) L. Wang, A. Menakath, F. Han, Y. Wang, P. Y. Zavalij, K. J. Gaskell, O. Borodin, D. Iuga, S. P. Brown, C. Wang, K. Xu, B. W. Eichhorn, *Nat. Chem.*

[8] **2019**, *11*, 789; b) W. M. Dose, W. Li, I. Temprano, C. A. O'Keefe, B. L. Mehdi, M. F. L. De Volder, C. P. Grey, *ACS Energy Lett.* **2022**, *7*, 3524.

[8] X. Xie, E. W. Clark Spotte-Smith, M. Wen, H. D. Patel, S. M. Blau, K. A. Persson, *J. Am. Chem. Soc.* **2021**, *143*, 13245.

[9] X. He, D. Bresser, S. Passerini, F. Baakes, U. Krewer, J. Lopez, C. T. Mallia, Y. Shao-Horn, I. Cekic-Laskovic, S. Wiemers-Meyer, F. A. Soto, V. Ponce, J. M. Seminario, P. B. Balbuena, H. Jia, W. Xu, Y. Xu, C. Wang, B. Horstmann, R. Amine, C.-C. Su, J. Shi, K. Amine, M. Winter, A. Latz, R. Kostecki, *Nat. Rev. Mater.* **2021**, *6*, 1036.

[10] a) N. Tsiouvaras, S. Meini, I. Buchberger, H. A. Gasteiger, *J. Electrochem. Soc.* **2013**, *160*, A471; b) B. Zhang, M. Metzger, S. Solchenbach, M. Payne, S. Meini, H. A. Gasteiger, A. Garsuch, B. L. Lucht, *J. Phys. Chem. C* **2015**, *119*, 11337; c) A. Guéguen, D. Streich, M. He, M. Mendez, F. F. Chesneau, P. Novák, E. J. Berg, *J. Electrochem. Soc.* **2016**, *163*, A1095; d) C. Bolli, A. Guéguen, M. A. Mendez, E. J. Berg, *Chem. Mater.* **2019**, *31*, 1258; e) C. Misiewicz, R. Lundström, I. Ahmed, M. J. Lacey, W. R. Brant, E. J. Berg, *J. Power Sources* **2023**, *554*, 232318.

[11] a) R. Imhof, P. Novák, *J. Electrochem. Soc.* **1998**, *145*, 1081; b) M. Winter, R. Imhof, F. Joho, P. Novák, *J. Power Sources* **1999**, *81–82*, 818; c) P. Novák, F. Joho, R. Imhof, J.-C. Panitz, O. Haas, *J. Power Sources* **1999**, *81–82*, 212; d) P. Novák, J.-C. Panitz, F. Joho, M. Lanz, R. Imhof, M. Coluccia, *J. Power Sources* **2000**, *90*, 52; e) B. B. Berkes, A. Jozwiuk, M. Vračar, H. Sommer, T. Brezesinski, J. Janek, *Anal. Chem.* **2015**, *87*, 5878.

[12] a) M. He, E. Castel, A. Laumann, G. Nuspl, P. Novák, E. J. Berg, *J. Electrochem. Soc.* **2015**, *162*, A870; b) M. Metzger, B. Strehle, S. Solchenbach, H. A. Gasteiger, *J. Electrochem. Soc.* **2016**, *163*, A798–A809; c) R. Jung, P. Strobl, F. Maglia, C. Stinner, H. A. Gasteiger, *J. Electrochem. Soc.* **2018**, *165*, A2869; d) K. N. Shitaw, S. C. Yang, S. K. Jiang, C. J. Huang, N. A. Sahalie, Y. Nikodimos, H. H. Weldeyohannes, C. H. Wang, S. H. Wu, W. N. Su, B. J. Hwang, *Adv. Funct. Mater.* **2021**, *31*, 2006951.

[13] W. Weber, R. Wagner, B. Streipert, V. Kraft, M. Winter, S. Nowak, *J. Power Sources* **2016**, *306*, 193.

[14] a) W. Weber, V. Kraft, M. Grützke, R. Wagner, M. Winter, S. Nowak, *J. Chromatogr. A* **2015**, *1394*, 128; b) I. Belharouak, G. M. Koenig, T. Tan, H. Yumoto, N. Ota, K. Amine, *J. Electrochem. Soc.* **2012**, *159*, A1165; c) D. J. Xiong, R. Petibon, M. Nie, L. Ma, J. Xia, J. R. Dahn, *J. Electrochem. Soc.* **2016**, *163*, A546.

[15] C. Schultz, S. Vedder, B. Streipert, M. Winter, S. Nowak, *RSC Adv.* **2017**, *7*, 27853.

[16] a) J. Diekmann, S. Doose, S. Weber, S. Münch, W. Haselrieder, A. Kwade, *J. Electrochem. Soc.* **2020**, *167*, 090504; b) B. B. Berkes, A. Jozwiuk, H. Sommer, T. Brezesinski, J. Janek, *Electrochem. Commun.* **2015**, *60*, 64; c) N. Schlüter, P. Novák, D. Schröder, *Adv. Energy Mater.* **2022**, *12*, 2200708.

[17] S. Solchenbach, M. Metzger, M. Egawa, H. Beyer, H. A. Gasteiger, *J. Electrochem. Soc.* **2018**, *165*, A3022–A3028.

[18] X. Tian, Y. Yi, B. Fang, P. Yang, T. Wang, P. Liu, L. Qu, M. Li, S. Zhang, *Chem. Mater.* **2020**, *32*, 9821.

[19] F. Baakes, M. Lüthe, M. Gerasimov, F. Laue, F. Röder, P. B. Balbuena, U. Krewer, *J. Power Sources* **2022**, *522*, 230881.

[20] S. Klein, J. M. Wrogemann, S. van Wickeren, P. Harte, P. Bärmann, B. Heidrich, J. Hesper, K. Borzutzki, S. Nowak, M. Börner, M. Winter, J. Kasnatscheew, T. Placke, *Adv. Energy Mater.* **2022**, *12*, 2102599.

[21] D. Parikh, C. J. Jafta, B. P. Thapaliya, J. Sharma, H. M. Meyer, C. Silkowski, J. Li, *J. Power Sources* **2021**, *507*, 230259.

[22] S. L. Dreyer, A. Kondrakov, J. Janek, T. Brezesinski, *J. Mater. Res.* **2022**, *37*, 3146.

[23] a) P. Novák, D. Goers, L. Hardwick, M. Holzapfel, W. Scheifele, A. Würsig, *J. Power Sources* **2005**, *146*, 15; b) J. Vetter, M. Holzapfel, A. Wuersig, W. Scheifele, J. Ufheil, P. Novák, *J. Power Sources* **2006**, *159*, 277; c) R. Lundström, E. J. Berg, *J. Power Sources* **2021**, *485*, 229347; d) M. Metzger, C. Marino, J. Sicklinger, D. Haering, H. A. Gasteiger, *J. Electrochem. Soc.* **2015**, *162*, A1123.

[24] Y. Abdul-Quadir, T. Laurila, J. Karppinen, K. Jalkanen, K. Vuorilehto, L. Skogström, M. Paulasto-Kröckel, *Int. J. Energy Res.* **2014**, *38*, 1424.

[25] B. S. Parimalam, A. D. MacIntosh, R. Kadam, B. L. Lucht, *J. Phys. Chem. C* **2017**, *121*, 22733.

[26] B. B. Berkes, A. Schiele, H. Sommer, T. Brezesinski, J. Janek, *J. Solid State Electrochem.* **2016**, *20*, 2961.

[27] X. Kong, Y. Zheng, M. Ouyang, L. Lu, J. Li, Z. Zhang, *J. Power Sources* **2018**, *395*, 358.

[28] S. Buechele, A. Adamson, A. Eldesoky, T. Boetticher, L. Hartmann, T. Boulanger, S. Azam, M. B. Johnson, T. Taskovic, E. Logan, M. Metzger, *J. Electrochem. Soc.* **2023**, *170*, 010511.

Batteries & Supercaps

Research Article
doi.org/10.1002/batt.202300534

Chemistry Europe
European Chemical
Societies Publishing

[29] a) S. Venkatachalam, S. G. Nayak, J. V. Labde, P. R. Gharal, K. Rao, A. K. Kelkar, in *Polyester* (Ed.: H. E.-D. Saleh), InTech, **2012**, 75; b) J. Scheirs, *Wiley series in polymer science*, Wiley, Chichester, **2003**, 750.

[30] I. Marshall, A. Todd, *Trans. Faraday Soc.* **1953**, *49*, 67.

[31] B. J. Holland, J. N. Hay, *Polymer* **2002**, *43*, 1835.

[32] a) R. Padhye, A. J. A. Aquino, D. Tunega, M. L. Pantoya, *ACS Appl. Mater. Interfaces* **2017**, *9*, 24290; b) Y. Lee, C. Huffman, S. M. George, *Chem. Mater.* **2016**, *28*, 7657; c) A. M. Cano, A. E. Marquardt, J. W. DuMont, S. M. George, *J. Phys. Chem. C* **2019**, *123*, 10346; d) E. R. Østli, Y. Tesfamhret, S. Wenner, M. J. Lacey, D. Brandell, A. M. Svensson, S. M. Selbach, N. P. Wagner, *ACS Omega* **2021**, *6*, 30644.

[33] a) R. Bernhard, M. Metzger, H. A. Gasteiger, *J. Electrochem. Soc.* **2015**, *162*, A1984; b) P. G. Kitz, M. J. Lacey, P. Novák, E. J. Berg, *J. Power Sources* **2020**, *477*, 228567.

[34] M. Metzger, B. Strehle, S. Solchenbach, H. A. Gasteiger, *J. Electrochem. Soc.* **2016**, *163*, A798.

[35] F. Baakes, D. Witt, U. Krewer, *Chem. Sci.* **2023**, *14*, 13783.

[36] L. Bläubaum, F. Röder, C. Nowak, H. S. Chan, A. Kwade, U. Krewer, *ChemElectroChem* **2020**, *7*, 4755.